Transient absorption spectroscopy and quantum-chemical studies of matrix-isolated perylene derivatives

E. Engel,[1] K. Schmidt,[2] D. Beljonne,[2,3] J.-L. Brédas,[2] J. Assa,[1] H. Fröb,[1] K. Leo,[1] and M. Hoffmann[1,*]
[1]*Institut für Angewandte Photophysik, Technische Universität Dresden, D-01062 Dresden, Germany*
[2]*School of Chemistry and Biochemistry and Center for Organic Photonics and Electronics, Georgia Institute of Technology, Atlanta, Georgia 30332-0400, USA*
[3]*Service de Chimie des Matériaux Nouveaux, Centre de Recherche en Electronique et Photonique Moléculaires, Université de Mons-Hainaut, B-7000 Mons, Belgium*

(Received 25 November 2005; published 29 June 2006)

We present a comprehensive experimental and theoretical study of the optical properties of matrix-isolated molecules of the two perylene derivatives N,N'-dimethylperylene-3,4,9,10-dicarboximide (MePTCDI) and 3,4,9,10-perylenetetracarboxylic dianhydride (PTCDA). A solid solution of the dyes in an SiO_2 matrix exhibits monomer-like behavior. Transient absorption pump-probe spectroscopy in the range 1.2–2.6 eV has been performed on an ultrafast time scale. The differential transmittance reveals contributions from ground-state bleaching, stimulated emission, and excited-state absorption. Both systems exhibit broad excited-state absorption features below 2.0 eV with a clear peak around 1.8 eV. The spectra can be consistently explained by the results of quantum-chemical calculations. We have applied both the coupled cluster singles and doubles (CCSD) model and the multireference-determinant single and double configuration-interaction (MRD-CI) technique on the basis of the intermediate neglect of differential overlap (INDO) Hamiltonian. The results are insensitive to whether the geometry is optimized for the electronic ground state or first excited state. The experimental polarization anisotropies for the two major transitions are in agreement with the calculated polarizations.

DOI: 10.1103/PhysRevB.73.245216 PACS number(s): 78.55.Kz, 71.35.−y, 71.15.−m, 78.47.+p

I. INTRODUCTION

Among the promising classes of novel organic materials suitable for applications in low-cost optoelectronic devices, substances forming quasi-one-dimensional (1D) molecular crystals have recently attracted considerable interest. Strong intermolecular orbital overlap, resulting in intense electronic coupling along one lattice direction, provides thin films with increased carrier mobility. Numerous contributions have focused on investigations of the structural, electronic, and optical properties of quasi-1D perylene derivatives; prominent among these are 3,4,9,10-perylenetetracarboxylic dianhydride (PTCDA) and N,N'-dimethylperylene-3,4,9,10-dicarboximide (MePTCDI),[1,2] see Fig. 1 for the chemical structures. However, knowledge about the initial relaxation processes after photoexcitation in these materials is still scarce, especially on an ultrafast time scale. Earlier works have addressed ultrafast excited-state dynamics in PTCDA by means of two-photon photoelectron spectroscopy[3] or transient absorption spectroscopy.[4–6] Yet, quantitative and reliable statements about the latter require a detailed analysis and thorough understanding of the optical transitions from the lowest exciton state (S_1) to higher excited states (S_n). In order to understand the structure of the higher excited states of the crystalline material, it is first necessary to clarify the properties of the isolated molecule.

A number of studies have already successfully addressed the molecular electronic properties of perylene derivatives, both experimentally[7–11] and theoretically.[12–15] The odd-symmetry electronically excited states of PTCDA have been well understood from linear spectroscopy, while virtually no information exists on the even-symmetry excited states, which are not observable in linear absorption spectroscopy. However, such an information is a prerequisite for the understanding of excited-state dynamics based on ultrafast nonlinear spectroscopy.

In this work, we report on femtosecond transient absorption spectra of matrix-isolated molecules of PTCDA and MePTCDI. We show that these spectra can be consistently explained by quantum-chemical calculations, which provide reliable estimates for both the energies of the excited states and the transition dipole moments among them. We have used the intermediate neglect of differential overlap (INDO) Hamiltonian together with the coupled cluster singles and doubles (CCSD) technique[16] and the multireference-determinant single and double configuration-interaction (MRD-CI) technique.[17] These methods have been demonstrated to provide excited-state energies and transition dipole moments in good agreement with experiment and to describe accurately excited-state absorption[18] and nonlinear optical processes such as two-photon absorption[19–22] and third-harmonic generation[20,21] in conjugated molecules. To account for geometrical relaxations of the molecules, calculations have been done for both the ground-state (S_0) and first-excited state (S_1) geometries.

A particular experimental challenge in case of the perylene derivatives PTCDA and MePTCDI is their very low solubility. It has been shown[7] that in solution, aggregates already form at concentrations lower than 1 μmol/L, which corresponds to a mean molecular distance of ~100 nm. This extremely hampers or even impedes measurements of nonlinear optical properties, for which high intensities in a strongly confined focus are required. One way to increase the concentration of molecules while still avoiding aggregation

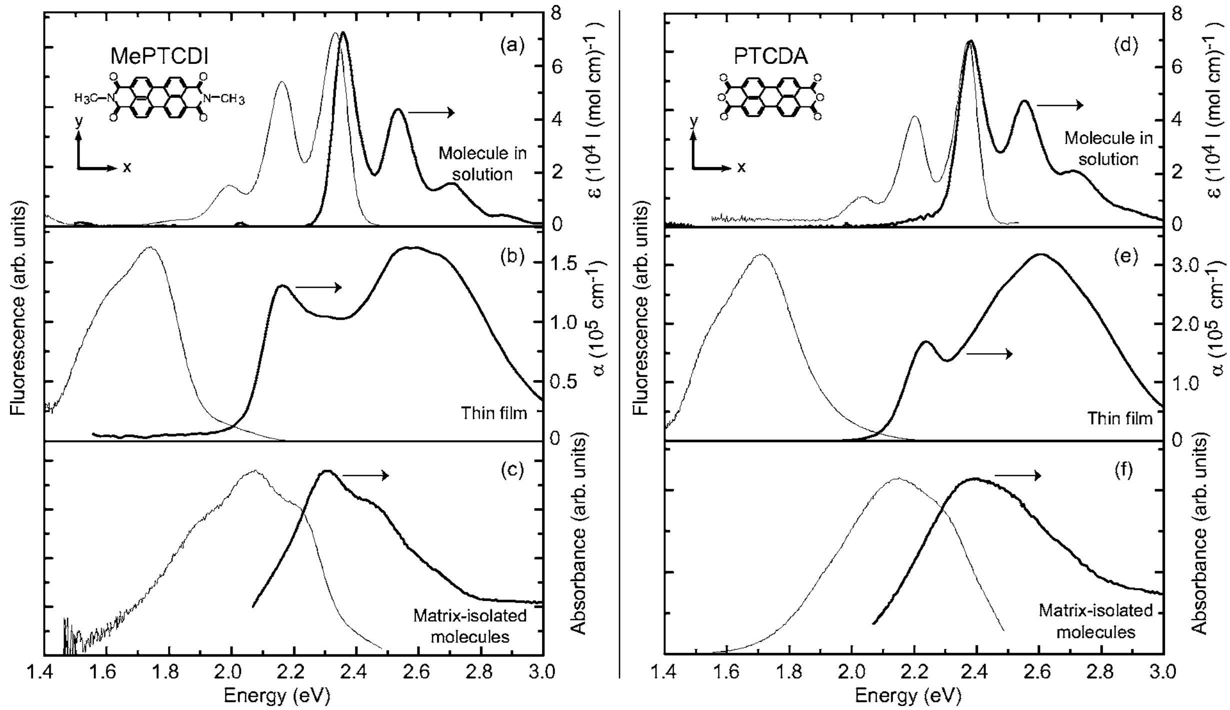

FIG. 1. Absorption and emission spectra of MePTCDI (a)–(c) and PTCDA (d)–(f) solutions, thin films, and matrix-isolated samples. Thick lines are absorption spectra and the thin lines are normalized emission spectra. In (a), the thick line is the molar extinction coefficient ε of MePTCDI in chloroform (0.3 μmol/1) (Ref. 8), and the thin line the emission spectrum of MePTCDI dissolved in chloroform (0.4 μmol/l). In (b), the absorption coefficient α of the MePTCDI thin film (Ref. 24) and emission from a thin film (35 nm on sapphire). The thick line in (c) shows the absorbance of the MePTCDI matrix sample, measured as cw fluorescence excitation. In (d), the thick line is the molar extinction coefficient ε of PTCDA in dimethyl sulfoxide (DMSO) (1.1 μmol/1) and the thin line the emission spectrum of PTCDA dissolved in chloroform (0.4 μmol/1). In (e), the absorption coefficient α of the PTCDA thin film (Ref. 25) and emission from a thin film (35 nm on sapphire). The thick line in (f) shows the absorbance of the PTCDA matrix sample, measured as cw fluorescence excitation. Insets depict the molecular structures and the molecular coordinate system. All data were taken at room temperature.

is to embed the molecules into a rigid matrix without any intermediate solution step. We therefore produced such solid solutions, where the dye was co-evaporated together with silicon oxide (SiO_2). A typical volume concentration of 1% results in an average molecular distance of about 3 nm, which is still 4.6 times larger than the mean distance in highly anisotropic polycrystalline films, and 9 times larger than the distance of adjacent molecules in the stacking direction.[1,23] With regard to the 1 μmol/L solution, the volume density is increased by a factor of about 5×10^4.

II. EXPERIMENTAL METHODS

Samples were prepared by co-evaporation of the organic dyes and SiO_2 under high vacuum (10^{-6} mbar) onto glass substrates. The dyes, purified by gradient sublimation, were evaporated from indirectly heated ceramic crucibles and SiO_2 was deposited by electron beam evaporation. The total sample thickness was 1.65 μm.

Linear absorption spectra of dissolved dyes (see Fig. 1) are given in absolute units. To obtain well-defined concentrations, the material was dissolved from vapor-deposited thin films as described in Ref. 8. We have reproduced here the absorption spectrum of MePTCDI in chloroform from Ref. 8 and give in addition the spectrum of PTCDA in dimethyl sulfoxide (DMSO). All fluorescence spectra are given in units of photons per energy interval. Absorption spectra of thin films are shown as absolute absorption coefficient α, which was determined from thin film optical models. The spectra are calculated from the optical constants given in Ref. 24 for MePTCDI and Ref. 25 for PTCDA.

Transient spectra were recorded with an ultrafast pump-probe setup pumped by a 1 kHz regenerative Ti:sapphire amplifier system. A fraction of the 790 nm output of 750 mW power pumped a home-built optical parametric amplifier in noncollinear geometry (N-OPA) (Ref. 26) with subsequent prism compressor. The linearly polarized output pulses were centered around 2.32 eV (535 nm) for MePTCDI and 2.39 eV (518 nm) for PTCDA, to excite the lowest vibronic state of the $S_0\rightarrow S_1$ transition (see Fig. 1). The probe pulses originated from a femtosecond continuum, ranging between 500 and 1020 nm, which was generated in a 2 mm sapphire plate. Spectral selection was performed after the sample with a monochromator with a stepwidth of 4 nm and a resolution of 3 nm. The data were recorded as differential transmission $\Delta T/T$, where ΔT is the pump-induced transmission change of the probe beam. For a better signal-to-noise ratio, an autobalanced photoreceiver (Si-PIN photodiodes) with a reference beam and lock-in detection at the laser frequency was employed. A broadband half waveplate allowed to rotate the polarization of the pump beam by 90° to determine the

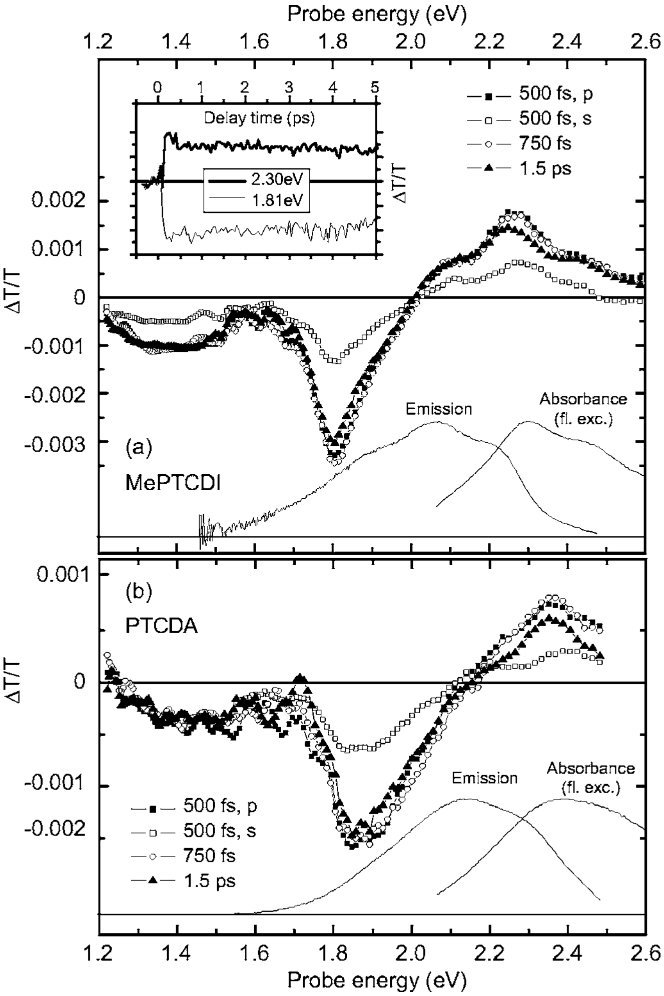

FIG. 2. Transient spectra of MePTCDI (a) and PTCDA (b) for probe pulse delays of 500 fs, 750 fs, and 1.5 ps. Probe polarization was parallel to pump polarization, except for open squares (pump and probe beam polarizations perpendicular). Thin solid lines are fluorescence excitation and emission spectra as in Fig. 1. Inset in (a), pump-probe traces as a function of delay for probe energies of 2.3 and 1.81 eV.

pump-probe anisotropy. The measurements were carried out at room temperature.

The zero position of the time axis had to be adjusted manually. This is due to the fact that the probe pulse gets chirped upon white-light generation. The zero position $\tau_0(\lambda)$ for the white light spectrum was calibrated in the following way: A neat SiO_2 matrix of 1 μm thickness on a glass substrate served as reference sample. During pulse overlap, a coherence spike could be detected, which allowed us to record $\tau_0(\lambda)$. The accuracy of this temporal calibration was about 200 fs, and the transient spectra presented below were calibrated accordingly.

III. EXPERIMENTAL RESULTS AND DISCUSSION

Figure 1 shows absorption and emission spectra of our samples in comparison with spectra of the molecules in solution and thin polycrystalline films. The corresponding S_1 state in PTCDA has been well investigated theoretically.[12–15] It has been shown that the transition dipole for the $S_0 \rightarrow S_1$ absorption is oriented along the long molecular axis of the molecule, which in our coordinate system corresponds to the x axis. The vibrational progression exhibits three distinct peaks with separations of 170 meV; such a progression can often be described by an effective internal vibrational mode,[27] which takes account of an ensemble of broadened vibrational substructures.[9,10,14]

Since the small signal is completely dominated by thin-film interferences from the SiO_2 matrix, the absorbance of the matrix-isolated samples was measured as fluorescence excitation spectrum. For MePTCDI, the spectrum in Fig. 1(c) clearly resembles the absorption spectrum of the molecule in solution. In particular, the peak at 2.30 eV and the shoulder at 2.47 eV are 170 meV apart. The emission spectrum also shows a substructure pointing towards single molecule behavior. The spectral broadening and the energetic shift may be caused by interaction with the solvent environment. In the case of the absorption and emission spectra of the PTCDA matrix system in Fig. 1(f), these distinct features are still visible, but less pronounced, which might indicate beginning of aggregation. However, the shape is clearly closer to the solvent spectrum than to the thin film spectrum. Since the in-stack interactions of two molecules, as seen in OMBE-grown films of two-monolayer thickness, leads to absorption spectra similar to the film spectrum,[28] it can be concluded that the spectra for the PTCDA/SiO_2 samples exhibit dominant monomer character. However, the absolute fraction of truly isolated molecules cannot be derived from the fluorescence emission or excitation spectra since quantum yields and energy transfer processes are not known. A direct proof of the dominantly monomeric nature of the samples is only given by the monomeric shape of ground state bleaching and the occurence and shape of stimulated emission in the transient spectra (see below).

Figure 2 shows the results of the pump-probe measurements. Initially, we recorded $\Delta T/T$ for several selected probe energies as a function of delay τ between pump and probe pulses. Two representative traces are shown in the small inset of Fig. 2(a). The signals $|\Delta T/T|$ reach their maxima after about 300 fs, and the subsequent decay (not shown) happens on a $\sim$50 ps time scale. The transient spectra have been corrected for chirp as described in the experimental section. To avoid possible signal contributions from a coherence regime during pulse overlap or initial relaxation, only spectra at delays of 500 fs or longer are presented. We assume that after 500 fs the geometry of the excited molecule has already relaxed into some equilibrated state. Vibrational relaxation times below 400 fs have been reported for similar perylene derivatives.[29]

In Fig. 2(a), the transient spectrum of MePTCDI is depicted as a function of the probe beam energy, at probe delays of 500 fs, 750 fs, and 1.5 ps. No significant changes can be recognized in the shape of the spectra with time, which implies that we are observing a single state, i.e., the excitation does not cross over multiple states during that period.

In general, the transient transmittance signal is a sum of three contributions: ground state bleaching [(GSB), related to a change of the linear absorption coefficient α], stimulated emission (SE), and excited-state absorption (ESA). As can be seen from Fig. 2(a), the shape of the $\Delta T/T$ signal above 2.20 eV resembles closely the shape of the linear absorbance, which is shown again in the panel. Therefore, we attribute the major signal contribution in this region to GSB. A closer look reveals that the maximum differential transmittance $\Delta T/T$ lies at 2.26 eV, whereas the absorbance maximum occurs at 2.30 eV. This energetic shift can be understood when considering that stimulated emission is also present in the signal: Due to Stokes shift, the $S_{1,0}\rightarrow S_{0,0}$ transition between the lowest excited state (zero-phonon state $S_{1,0}$) and the zero-phonon ground state $S_{0,0}$ lies at 2.21 eV and is seen as a shoulder in the emission spectrum. This transition will also be probed as transient stimulated emission, and the stimulated emission contribution should appear in the $\Delta T/T$ signal with its maximum at 2.21 eV. The observed peak at 2.26 eV thus arises from the fact that we see a superposition of both GSB and SE. Additionally, a shoulder in the transient transmittance shows up at 2.08 eV and corresponds nicely to the $S_{1,0}\rightarrow S_{0,1}$ peak of the emission spectrum. Hence, we assign this feature to stimulated emission back to the one-phonon ground state.

The observation of SE is an indication that the transient transmittance signal does mainly come from isolated molecules: In the case of an aggregated crystalline sample, MePTCDI has a negative exciton dispersion in k-space[30,31] and the relaxation time for the depopulation of the absorbing state at the Γ-point towards the border of the Brillouin zone is on the order of 100 fs.[5,6] In this case, SE from the border of the Brillouin zone would occur with a strongly reduced cross section because of the indirect transition and it would have a very different spectrum corresponding to the photoluminescence spectrum of an aggregate or film [see Fig. 1(b)]. Indeed, the transient absorption spectrum of an actual thin film (shown in Ref. 5) looks significantly different and does not show the characteristic monomer features in the GSB and SE signal, and also the ESA peak at around 1.8 eV (see below) is much broader in the film than in the matrix-isolated samples. Thus, our transient spectra can be clearly related to isolated molecules.

At energies below ~2.0 eV, the transient spectrum exhibits one pronounced peak around 1.81 eV and a broad structure around 1.38 eV, both with negative $\Delta T/T$. This can be interpreted as ESA from S_1 into higher states of even symmetry, which are dipole-forbidden from the ground state. While the main peak at 1.81 eV is rather narrow, the second peak is broad.

In addition to the energy of the excited states, we can evaluate the polarization of the transition dipole moments. The pump-probe anisotropy can be defined in accordance to the fluorescence anisotropy,[32] i.e.,

$$r(t)=\frac{I_p-I_s}{I_p+2I_s}, \tag{1}$$

where I_p and I_s are $\Delta T/T$ signals parallel and perpendicular to the linearly polarized excitation, respectively. In pump-probe, we first create a population in S_1 which is proportional to the square of the projection of the transition dipole moment $\mathbf{p}_1$ for absorption onto the pump electric field. The

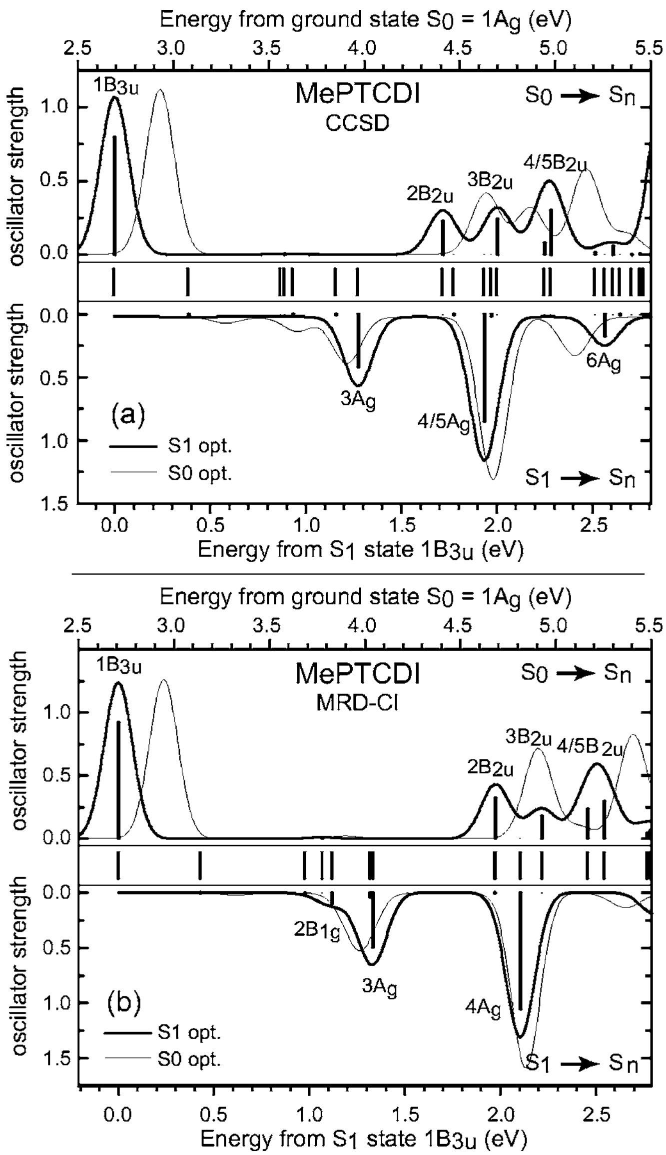

FIG. 3. Quantum-chemical calculations of the MePTCDI single molecule: CCSD method (a) and MRD-CI technique (b). Upper frames show the absorption from the ground state S_0 ($1A_g$), and lower frames display the absorption from the lowest excited state S_1 ($1B_{3u}$). Energies and oscillator strengths are only displayed for the $1B_{3u}$ geometry. The lines are convolutions with Gaussians of 175 meV FWHM. Thick lines: $1B_{3u}$ geometry, thin lines for comparison: $1A_g$ geometry. All labels refer to the D_{2h} symmetry of the MePTCDI backbone. Note that for the $S_1\rightarrow S_n$ transitions, the axis for the energy from the ground state (top tickmarks) is only valid for the S_1-optimized result.

probe beam probes either the same transition dipole (GSB and SE) or any transition dipole to higher states (ESA). Again, the signal is proportional to the square of the projection of the relevant transition dipole moment $\mathbf{p}_2$ to the probe polarization. Just as in fluorescence, the average over an isotropic sample results in an anisotropy of $r=0.4$ ($r=-0.2$) when the probed dipole is parallel (perpendicular) to the excited one. The open squares in Fig. 2(a) illustrate the mutually perpendicular orientation of pump and probe polarizations at 500 fs delay while the solid squares correspond to

TABLE I. Symmetry label, state energy, oscillator strength, and polarization for the first 20 electronic states above the lowest excited state for the MePTCDI molecule classified by calculation method and by geometry; $f(S_0)$ and $f(S_1)$ are the oscillator strength from the ground state S_0 and the S_1 state, respectively. All symmetry labels refer to the D_{2h} symmetry of the MePTCDI backbone.

CCSD								MRD-CI							
S_1 geometry				S_0 geometry				S_1 geometry				S_0 geometry			
Name	E(eV)	$f(S_0)$	$f(S_1)$	Name	E(eV)	$f(S_0)$	$f(S_1)$	Name	E(eV)	$f(S_0)$	$f(S_1)$	Name	E(eV)	$f(S_0)$	$f(S_1)$
$1A_g$	0			$1A_g$	0			$1A_g$	0			$1A_g$	0		
$1B_{3u}$	2.69	0.79(x)		$1B_{3u}$	2.93	0.83(x)		$1B_{3u}$	2.71	0.92(x)		$1B_{3u}$	2.95	0.94(x)	
$2A_g$	3.08	0	$<10^{-2}$	$2A_g$	3.51	0	0.04(x)	$2A_g$	3.14	0	$<10^{-2}$	$2A_g$	3.57	0	0.02(x)
$1B_{1g}$	3.56	0	$<10^{-2}$	$1B_{1g}$	3.70	0	$<10^{-2}$	$1B_{1g}$	3.69	0	0.01(y)	$1B_{1g}$	3.80	0	$<10^{-2}$
$1B_{2u}$	3.58	$<10^{-2}$	0	$1B_{2u}$	3.72	0.01(y)	0	$1B_{2u}$	3.78	0.01(y)	0	$1B_{2u}$	3.90	0.02(y)	0
$2B_{1g}$	3.63	0	$<10^{-2}$	$2B_{1g}$	3.89	0	0.09(y)	$2B_{1g}$	3.83	0	0.09(y)	$2B_{1g}$	4.16	0	0.12(y)
$3B_{1g}$	3.85	0	$<10^{-2}$	$3B_{1g}$	4.11	0	0.02(y)	$3B_{1g}$	4.03	0	0.04(y)	$3A_g$	4.23	0	0.34(x)
$3A_g$	3.97	0	0.41(x)	$3A_g$	4.15	0	0.26(x)	$3A_g$	4.04	0	0.49(x)	$3B_{1g}$	4.29	0	$<10^{-2}$
$2B_{2u}$	4.41	0.22(y)	0	$4B_{1g}$	4.62	0	$<10^{-2}$	$4B_{1g}$	4.68	0	$<10^{-2}$	$4B_{1g}$	4.79	0	$<10^{-2}$
$4B_{1g}$	4.47	0	$<10^{-2}$	$2B_{2u}$	4.64	0.31(y)	0	$2B_{2u}$	4.68	0.32(y)	0	$2B_{2u}$	4.91	0.53(y)	0
$4A_g$	4.63	0	0.85(x)	$3B_{2u}$	4.87	0.24(y)	0	$4A_g$	4.81	0	1.05(x)	$4A_g$	5.08	0	1.27(x)
$5A_g$	4.67	0	0.01(x)	$4A_g$	4.91	0	0.97(x)	$3B_{2u}$	4.93	0.18(y)	0	$3B_{2u}$	5.12	0.07(y)	0
$3B_{2u}$	4.70	0.24(y)	0	$5A_g$	4.99	0	$<10^{-2}$	$4B_{2u}$	5.17	0.23(y)	0	$4B_{2u}$	5.40	0.13(y)	0
$4B_{2u}$	4.95	0.08(y)	0	$4B_{2u}$	5.16	0.43(y)	0	$5B_{2u}$	5.25	0.29(y)	0	$5B_{2u}$	5.41	0.48(y)	0
$5B_{2u}$	4.98	0.30(y)	0	$5B_{2u}$	5.22	$<10^{-2}$	0	$2B_{3u}$	5.48	0.04(x)	0	$2B_{3u}$	5.54	0.01(x)	0
$2B_{3u}$	5.21	0.01(x)	0	$2B_{3u}$	5.29	0.01(x)	0	$6B_{2u}$	5.49	0.06(y)	0	$5B_{1g}$	5.55	0	0.02(y)
$6A_g$	5.26	0	0.17(x)	$6A_g$	5.34	0	0.22(x)	$5A_g$	5.50	0	0.11(x)	$6B_{2u}$	5.57	0.04(y)	0
$6B_{2u}$	5.30	0.06(y)	0	$6B_{2u}$	5.38	0.10(y)	0	$3B_{3u}$	5.68	$<10^{-2}$	0	$5A_g$	5.61	0	0.09(x)
$5B_{1g}$	5.34	0	$<10^{-2}$	$5B_{1g}$	5.40	0	0.02(y)	$7B_{2u}$	5.81	0.05(y)	0	$3B_{3u}$	5.95	0.03(x)	0
$3B_{3u}$	5.40	$<10^{-2}$	0	$3B_{3u}$	5.57	$<10^{-2}$	0	$4B_{3u}$	5.87	1.05(x)	0	$7B_{2u}$	6.07	0.03(y)	0
$4B_{3u}$	5.44	$<10^{-2}$	0	$4B_{3u}$	5.72	0.03(x)	0	$8B_{2u}$	5.96	0.28(y)	0	$4B_{3u}$	6.14	0.79(x)	0
$6B_{1g}$	5.47	0	$<10^{-2}$	$5B_{3u}$	5.79	0.89(x)	0	$6B_{1g}$	5.99	0	0.01(y)	$6B_{1g}$	6.20	0	0.02(y)

the parallel orientation. For the peak at 2.26 eV, one obtains from Eq. (1) $r=0.32\pm0.03$. In the case of GSB and SE, pump and probe transition dipoles have the same orientation and one would expect $r=0.4$. Nevertheless, the experimental value is close to it and clearly not $r=-0.2$. The D_{2h} symmetry (of the molecular backbone) limits the orientation for any probe transition dipole $\mathbf{p}_2$ to $\mathbf{p}_1 \parallel \mathbf{p}_2$ or $\mathbf{p}_1 \perp \mathbf{p}_2$. Therefore, it can be concluded that even though the measured anisotropy value does not fully coincide with the expected one, the transition dipoles possess the same polarization (x) and are oriented along the long axis of the MePTCDI molecule (see Fig. 1), in agreement with the assignment of GSB and SE. The ESA peak at 1.81 eV has an anisotropy $r=0.33\pm0.02$, which also points to the fact that the $S_1 \rightarrow S_n$ transition (where S_n is the state in question) is x-polarized. The anisotropies reported here do not change significantly with time.

The transient absorption spectrum $\Delta T/T$ for the PTCDA matrix sample in Fig. 2(b) looks very similar to the one of MePTCDI. Again, the general shape of the spectra does not vary with time, except for slight variations which can be explained by the overall reduction in signal-to-noise ratio. In accordance with MePTCDI, the maxima of the absorbance at 2.39 eV and of the transient transmittance at 2.35 eV do not coincide. The $S_{1,0} \rightarrow S_{0,0}$ transition now lies at 2.29 eV, i.e., the Stokes shift is of the same order as for MePTCDI. A SE contribution from the $S_{1,0} \rightarrow S_{0,0}$ transition could also explain the shift between the maxima of $\Delta T/T$ and the absorbance, as in the case of MePTCDI. However, there is no such distinct shoulder for stimulated emission from the $S_{1,0} \rightarrow S_{0,1}$ transition.

In general, the transient absorption spectrum of our PTCDA sample resembles recently observed thin film spectra:[6] In contrast to MePTCDI, the peaks are broader, which again might be related to beginning of aggregation in the sample. This fact also holds for the main ESA peak $S_1 \rightarrow S_n$, which now lies around 1.87 eV with a small broad feature around 1.43 eV. The signal-to-noise ratio did not allow a determination of the perpendicular orientation at 500 fs below 1.5 eV. For PTCDA, the pump-probe anisotropies evaluate to $r=0.35\pm0.13$ for the GSB and SE peak at 2.35 eV and $r=0.35\pm0.07$ for the main ESA peak at 1.87 eV. For the latter, this result gives evidence that this prominent $S_1 \rightarrow S_n$ transition is also x-polarized, as in MePTCDI.

TABLE II. Symmetry label, state energy, oscillator strength and polarization for the first 20 electronic states above the lowest excited state for the PTCDA molecule classified by calculation method and by geometry; $f(S_0)$ and $f(S_1)$ are the oscillator strength from the ground state S_0 and the S_1 state, respectively. All symmetry labels refer to the D_{2h} symmetry of the PTCDA molecule.

CCSD								MRD-CI							
S_1 geometry				S_0 geometry				S_1 geometry				S_0 geometry			
Name	E(eV)	$f(S_0)$	$f(S_1)$	Name	E(eV)	$f(S_0)$	$f(S_1)$	Name	E(eV)	$f(S_0)$	$f(S_1)$	Name	E(eV)	$f(S_0)$	$f(S_1)$
$1A_g$	0			$1A_g$	0			$1A_g$	0			$1A_g$	0		
$1B_{3u}$	2.74	0.78(x)		$1B_{3u}$	2.98	0.82(x)		$1B_{3u}$	2.75	0.90(x)		$1B_{3u}$	3.00	0.92(x)	
$2A_g$	3.09	0	$<10^{-2}$	$2A_g$	3.53	0	0.03(x)	$2A_g$	3.16	0	$<10^{-2}$	$2A_g$	3.59	0	0.01(x)
$1B_{1g}$	3.54	0	0.05(y)	$1B_{1g}$	3.72	0	0.01(y)	$1B_{1g}$	3.70	0	$<10^{-2}$	$1B_{1g}$	3.82	0	$<10^{-2}$
$1B_{2u}$	3.59	$<10^{-2}$	0	$1B_{2u}$	3.73	$<10^{-2}$	0	$1B_{2u}$	3.77	0.01(y)	0	$1B_{2u}$	3.90	0.01(y)	0
$2B_{1g}$	3.63	0	0.03(y)	$2B_{1g}$	3.84	0	0.07(y)	$2B_{1g}$	3.82	0	0.11(y)	$2B_{1g}$	4.11	0	0.10(y)
$3B_{1g}$	3.93	0	0.02(y)	$3B_{1g}$	4.20	0	0.04(y)	$3B_{1g}$	4.08	0	0.01(y)	$3A_g$	4.28	0	0.33(x)
$3A_g$	4.02	0	0.41(x)	$3A_g$	4.21	0	0.27(x)	$3A_g$	4.09	0	0.50(x)	$3B_{1g}$	4.36	0	0.03(y)
$2B_{2u}$	4.34	0.21(y)	0	$2B_{2u}$	4.55	0.24(y)	0	$2B_{2u}$	4.63	0.32(y)	0	$4B_{1g}$	4.83	0	$<10^{-2}$
$4B_{1g}$	4.50	0	$<10^{-2}$	$4B_{1g}$	4.67	0	$<10^{-2}$	$4B_{1g}$	4.69	0	$<10^{-2}$	$2B_{2u}$	4.86	0.47(y)	0
$4A_g$	4.64	0	0.08(x)	$3B_{2u}$	4.91	0.63(y)	0	$4A_g$	4.83	0	0.95(x)	$3B_{2u}$	5.10	0.43(y)	0
$5A_g$	4.65	0	0.73(x)	$4A_g$	4.93	0	0.83(x)	$3B_{2u}$	4.93	0.45(y)	0	$4A_g$	5.11	0	1.15(x)
$3B_{2u}$	4.74	0.54(y)	0	$5A_g$	4.97	0	0.02(x)	$4B_{2u}$	5.17	0.15(y)	0	$4B_{2u}$	5.43	0.23(y)	0
$4B_{2u}$	4.92	0.04(y)	0	$4B_{2u}$	5.18	0.04(y)	0	$1B_{1u}$	5.43	$<10^{-2}$	0	$2B_{3u}$	5.49	0.01(x)	0
$1B_{1u}$	5.15	$<10^{-2}$	0	$2B_{3u}$	5.24	0.01(x)	0	$2B_{3u}$	5.43	0.04(x)	0	$5B_{2u}$	5.55	0.04(y)	0
$2B_{3u}$	5.18	0.02(x)	0	$6A_g$	5.31	0	0.27(x)	$5B_{2u}$	5.47	0.08(y)	0	$5A_g$	5.58	0	0.12(x)
$6A_g$	5.23	0	0.19(x)	$1B_{1u}$	5.37	$<10^{-2}$	0	$5A_g$	5.50	0	0.11(x)	$5B_{1g}$	5.58	0	0.03(y)
$5B_{2u}$	5.32	0.05(y)	0	$5B_{2u}$	5.40	0.09(x)	0	$5B_{1g}$	5.53	0	0.06(y)	$6B_{1g}$	5.63	$<10^{-2}$	0
$5B_{1g}$	5.36	0	0.04(y)	$5B_{1g}$	5.43	0	0.02(y)	$3B_{3u}$	5.68	$<10^{-2}$	0	$3B_{3u}$	5.99	0.05(x)	0
$3B_{3u}$	5.40	$<10^{-2}$	0	$3B_{3u}$	5.57	$<10^{-2}$	0	$4B_{3u}$	5.87	1.07(x)	0	$4B_{3u}$	6.12	0.79(x)	0
$6B_{1g}$	5.41	0	$<10^{-2}$	$4B_{3u}$	5.73	0.39(x)	0	$6B_{2u}$	5.91	0.02(y)	0	$6B_{2u}$	6.13	0.01(y)	0
$4B_{3u}$	5.44	$<10^{-2}$	0	$5B_{3u}$	5.79	0.61(x)	0	$6B_{1g}$	5.93	0	$<10^{-2}$	$7B_{1g}$	6.20	0	0.01(y)

IV. QUANTUM-CHEMICAL RESULTS AND DISCUSSION

The assignment of the experimentally observed transitions can be done by means of highly correlated quantum-chemical methods. For the theoretical prediction of the excited states, two scenarios must be distinguished: In the first case, the probe pulse is considered to be absorbed prior to relaxation of the structure of the excited molecule. In the second case, the molecule is considered to rearrange and lower its energy prior to absorption of the probe pulse. To account for both situations, the excited states were obtained for molecules both adopting the structurally-relaxed geometries associated with the ground state S_0 ($1A_g$) and with the lowest excited state S_1 ($1B_{3u}$).

S_0 was optimized with density functional theory (DFT) and S_1 with time-dependent density functional theory (TDDFT),[33–35] using the B3LYP exchange-correlation functional[36] and the split valence basis set SV(P) (Ref. 37) as implemented in TURBOMOLE.[38–40] We evaluated the excited-state energies and transition dipole moments with the intermediate neglect of differential overlap (INDO/S) method[41] (using the Mataga-Nishimoto potential to describe Coulomb repulsion terms[42]) combined with two different schemes to include correlation effects: the coupled cluster method with singles and doubles[16,43] (CCSD) and the multireference double-configuration-interaction (MRD-CI) technique.[17,44] Both approaches incorporate higher excitations (i.e., doubly, triply, and quadruply excited configurations) that are necessary to provide more quantitative predictions. In particular, doubly excited determinants constitute a significant portion of the excited states that are active in two-photon absorption.[44–48]

In all methods, the molecular orbitals entering the active space of configuration interaction ranged from the six highest occupied to the six lowest unoccupied molecular orbitals. In the case of MRD-CI, those determinants that are dominant in the description of the ground state and the lowest excited states served in addition to the SCF-ground state determinant as references: The singly excited determinants highest occupied molecular orbital (HOMO)$\rightarrow$lowest unoccupied molecular orbital (LUMO), HOMO$\rightarrow$LUMO+1, HOMO$-$1$\rightarrow$LUMO, HOMO$-$1$\rightarrow$LUMO+1, and the doubly excited HOMO, HOMO$\rightarrow$LUMO, LUMO determinant. The same set of reference determinants was found necessary to reliably describe the excited states of other quadrupolar molecules.[22,49]

The result for the MePTCDI molecule is shown in Fig. 3, for both the CCSD method (a) and the MRD-CI technique (b). Numerical results are listed in Table I. The short vertical bars in the center of both panels illustrate the state energies

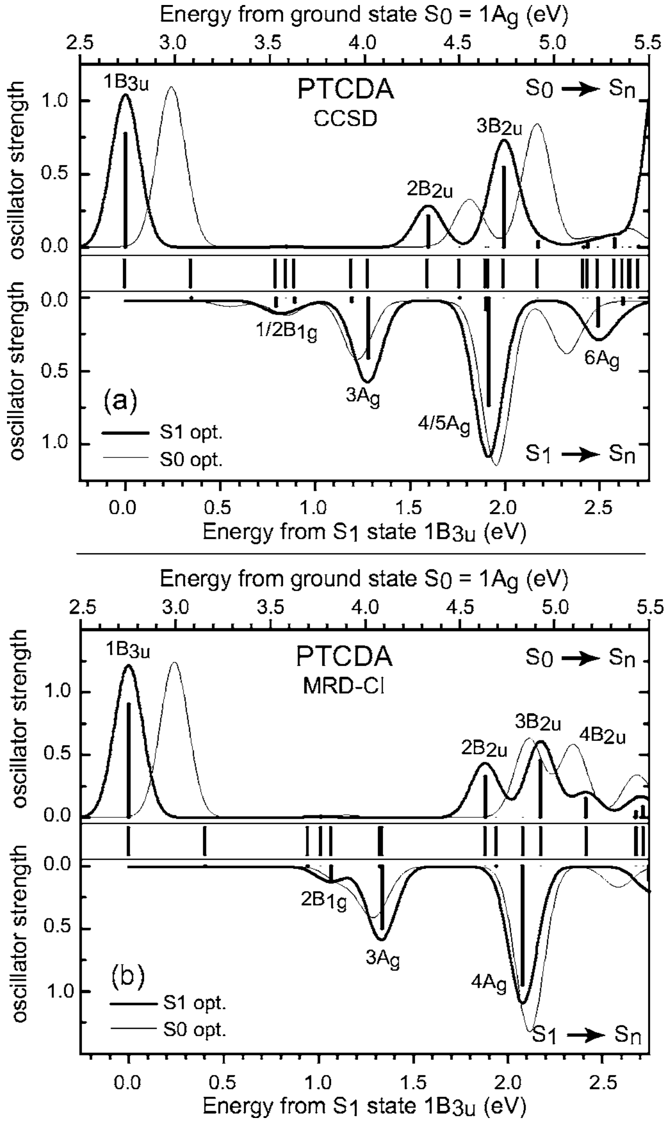

FIG. 4. Same as in Fig. 3, but for a PTCDA single molecule. Labels refer to the D_{2h} symmetry of PTCDA.

(based on the S_1-optimized geometry), either with respect to the ground state (top tickmarks) or with respect to the lowest excited S_1 state $1B_{3u}$ (bottom tickmarks). The long vertical bars display the oscillator strength of the respective transitions. The symmetry of the states can immediately be recognized: Odd-symmetry (ungerade) states are dipole-allowed from the even-symmetry (gerade) ground state, whereas even-symmetry (gerade) states are dipole-allowed from the odd-symmetry (ungerade) S_1 state.

The lines are convolutions of the states with Gaussians of 175 meV FWHM. For comparison, the thin lines represent identical convolutions of the respective states for the S_0-optimized geometry. The major transitions are labeled with the classification refering to the D_{2h} symmetry of the backbone shared by MePTCDI and PTCDA. Is is worth mentioning that we have not dealt in this work with the vibronic progression of the electronic states. With regard to ground-state absorption, the assumption that pumping reaches only into the S_1 state is justified, since the higher

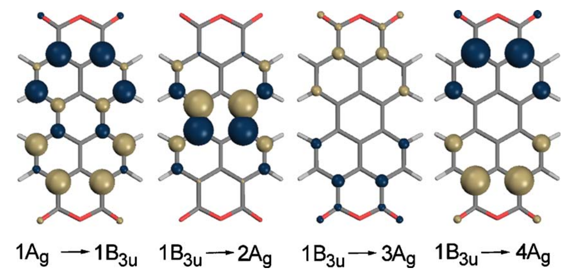

FIG. 5. (Color online) Transition densities of selected transitions in PTCDA in $1B_{3u}$ geometry (MRD-CI).

states starting with $1B_{2u}$ (refered to as the S_2 state in Ref. 8) are very well separated in energy.

The CCSD calculations for MePTCDI lead to three distinct ESA peaks located at energies 1.27 eV ($3A_g$), 1.93 eV ($4A_g$), and 2.57 eV ($6A_g$) above the $1B_{3u}$ state. The $4A_g$ state is accompanied by a small satellite $5A_g$ at 1.97 eV. In the case of calculations based on the S_0-optimized geometry, these values shift slightly, but the nature of the states does not change. All four transitions are x-polarized, i.e., the relevant transition dipole moment is parallel to the $S_0 \rightarrow S_1$ transition dipole moment. This implies a pump-probe anisotropy of $r=0.4$. Thus, we can correlate the $4A_g$ state to the experimentally observed peak at 1.81 eV. The energy difference between the $3A_g$ and $4A_g$ states is equal to 0.66 eV; we would thus expect the $3A_g$ state at about 1.14 eV, which is just beyond the range experimentally accessible with white light from sapphire and silicon photodetectors. The broad structure experimentally observed around 1.38 eV cannot be easily correlated to the calculations, however, as mentioned earlier, it might be attributed to the formation of aggregates, because a similar peak shows up in the transient spectra of thin films.[6,50] Considering the energy difference of 0.64 eV between the $4A_g$ and $6A_g$ states, we expect the latter to appear in the experiment around 2.45 eV. The transient spectra in Fig. 2(a) give no indication of an ESA peak in the accessible region up to 2.6 eV. Thus, the $6A_g$ state is either at higher energies or gives a much smaller oscillator strength than calculated.

Qualitatively, the results of the MRD-CI calculations reported in Fig. 3(b) are very similar to those of the CCSD calculations. The $3A_g$, $4A_g$, and $5A_g$ states have energies of 1.33, 2.10, and 2.81 eV, respectively, and all transitions from $1B_{3u}$ into them are x-polarized. However, the values obtained with the CCSD calculations are in better agreement with experiment. The results for the S_0-optimized geometry (thin lines in Fig. 3) are given for completeness. Since the ordering of the states and their associated oscillator strengths are essentially kept, independently of the adopted geometry, no distinction is possible between absorptions taking place from the structurally unrelaxed or fully relaxed S_1 state.

Figure 4 displays the result of the calculations for the PTCDA molecule. As for MePTCDI, the $S_1 \rightarrow S_n$ absorption in the CCSD calculations is dominated by three major peaks: $3A_g$ (1.28 eV), $5A_g$ (1.91 eV, with satellite $4A_g$, 1.90 eV), and $6A_g$ (2.49 eV), with energies relative to $1B_{3u}$. All these transitions are x-polarized and the experimental data are consistent with the results of the calculations. The MRD-CI calculations for PTCDA in Fig. 4(b) provide $3A_g$, $4A_g$, and $5A_g$ states with energies of 1.33, 2.08, and 2.74 eV, respectively. For the sake of completeness, the energies, oscillator strengths, and polarizations of the 21 lowest excited states are listed in Table II for PTCDA.

The major role of the transitions from $1B_{3u}$ into gerade states can be straight-forwardly explained by their polarization along the long molecular axis (x axis). Considering the shape of the molecule, the largest possible transition dipole moments can be formed along its long molecular axis. The transition densities corresponding to the excitations from $1B_{3u}$ into the lowest three gerade states are shown in Fig. 5, as well as the transition density associated to $1A_g \rightarrow 1B_{3u}$ for comparison. Since the transition density for the $1B_{3u} \rightarrow 2A_g$ transition is confined to the center of the molecule, the associated transition dipole moment is very small. In case $3A_g$ or $4A_g$ is the final state, the transition density spreads out over the whole molecule and, thus, gives rise to a large transition dipole moment. In both transitions, the same configurations participate with different mixing coefficients. The CI coefficients for $1B_{3u} \rightarrow 4A_g$ favor particularly large local contributions to the transition density that leads to a transition dipole moment comparable to the $1A_g \rightarrow 1B_{3u}$ transition.

V. CONCLUSION

In conclusion, we have presented time-resolved transient absorption spectra in the visible and near-IR spectral regions for matrix-isolated molecules of two perylene derivatives MePTCDI and PTCDA. By means of quantum-chemical calculations, we have been able to rationalize these spectra. The major transitions have been identified and the expected polarizations confirmed on the basis of the experimental pump-probe anisotropy. The theoretical results turn out to be relatively insensitive to either the method used (CCSD or MRD-CI) or the consideration of geometrical relaxation in the first excited state.

ACKNOWLEDGMENTS

Financial support by the Deutsche Forschungsgemeinschaft (Projects No. HA 3280/1, No. HO 2450/1, and DFG Leibnizpreis) at IAPP and the National Science Foundation (through the STC Program under Grant No. DMR-0120967, under Grant No. CHE-0342321, and under Grant No. CRIF 04-43564) and the Office of Naval Research at the Georgia Institute of Technology is gratefully acknowledged. D.B. is supported by the Belgian National Research Science Foundation.

*Email address: michael.hoffmann@iapp.de

[1] E. Hädicke and F. Graser, Acta Crystallogr., Sect. C: Cryst. Struct. Commun. **42**, 189 (1986).
[2] S. R. Forrest, Chem. Rev. (Washington, D.C.) **97**, 1793 (1997).
[3] D. Ino, K. Watanabe, N. Takagi, and Y. Matsumoto, Chem. Phys. Lett. **383**, 261 (2004).
[4] E. Engel, M. Koschorreck, K. Leo, and M. Hoffmann, J. Lumin. **112**, 299 (2005).
[5] E. Engel, M. Koschorreck, K. Leo, and M. Hoffmann, Phys. Rev. Lett. **95**, 157403 (2005).
[6] E. Engel, K. Leo, and M. Hoffmann, Chem. Phys. **325**, 170 (2006).
[7] V. Bulović, P. E. Burrows, S. R. Forrest, J. A. Cronin, and M. E. Thompson, Chem. Phys. **210**, 1 (1996).
[8] M. Hoffmann, K. Schmidt, T. Fritz, T. Hasche, V. M. Agranovich, and K. Leo, Chem. Phys. **258**, 73 (2000).
[9] M. Wewer and F. Stienkemeier, Phys. Rev. B **67**, 125201 (2003).
[10] M. Wewer and F. Stienkemeier, Phys. Chem. Chem. Phys. **7**, 1171 (2005).
[11] S. L. Oliveira, D. S. Corrêa, L. Misoguti, C. J. L. Constantino, R. F. Aroca, S. C. Zílio, and C. R. Mendonça, Adv. Mater. (Weinheim, Ger.) **17**, 1890 (2005).
[12] M. Sadrai, L. Hadel, R. R. Sauers, S. Husain, K. Krogh-Jespersen, J. D. Westbrook, and G. R. Bird, J. Phys. Chem. **96**, 7988 (1992).
[13] M. Adachi, Y. Murata, and S. Nakamura, J. Phys. Chem. **99**, 14240 (1995).
[14] R. Scholz, A. Y. Kobitski, T. U. Kampen, M. Schreiber, D. R. T. Zahn, G. Jungnickel, M. Elstner, M. Sternberg, and T. Frauenheim, Phys. Rev. B **61**, 13659 (2000).
[15] M. Makowski and M. T. Pawlikowski, Chem. Phys. Lett. **393**, 305 (2004).
[16] G. D. Purvis III and R. Bartlett, J. Chem. Phys. **76**, 1910 (1982).
[17] R. J. Buenker and S. D. Peyerimhoff, Theor. Chim. Acta **35**, 33 (1974).
[18] D. Beljonne, G. E. O'Keefe, P. J. Hamer, R. H. Friend, H. L. Anderson, and J. L. Brédas, J. Chem. Phys. **106**, 9439 (1997).
[19] M. Albota *et al.*, Science **281**, 1653 (1998).
[20] D. Beljonne, J. Cornil, Z. Shuai, J. L. Brédas, F. Rohlfing, D. D. C. Bradley, W. E. Torruellas, V. Ricci, and G. I. Stegeman, Phys. Rev. B **55**, 1505 (1997).
[21] D. Beljonne, Z. Shuai, J. Cornil, D. A. dos Santos, and J. L. Brédas, J. Chem. Phys. **111**, 2829 (1999).
[22] E. Zojer, D. Beljonne, T. Kogej, H. Vogel, S. R. Marder, J. W. Perry, and J. L. Brédas, J. Chem. Phys. **116**, 3646 (2002).
[23] A. J. Lovinger, S. R. Forrest, M. L. Kaplan, P. H. Schmidt, and T. Venkatesan, J. Appl. Phys. **55**, 476 (1984).
[24] A. B. Djurisic, T. Fritz, and K. Leo, Opt. Commun. **166**, 35 (1999).
[25] A. B. Djurisic, T. Fritz, and K. Leo, Opt. Commun. **183**, 123 (2000).
[26] T. Wilhelm, J. Piel, and E. Riedle, Opt. Lett. **22**, 1494 (1997).
[27] M. H. Hennessy, Z. G. Soos, R. A. Pascal Jr., and A. Girlando, Chem. Phys. **245**, 199 (1999).
[28] H. Proehl, T. Dienel, R. Nitsche, and T. Fritz, Phys. Rev. Lett. **93**, 097403 (2004).
[29] E. M. H. P. van Dijk, J. Hernando, J.-J. García-López, M. Crego-Calama, D. N. Reinhoudt, L. Kuipers, M. F. García-Parajó, and N. F. van Hulst, Phys. Rev. Lett. **94**, 078302 (2005).
[30] M. Hoffmann, Z. G. Soos, and K. Leo, Mol. Cryst. Liq. Cryst. Sci. Technol., Sect. B: Nonlinear Opt. **29**, 227 (2002).
[31] M. Hoffmann and Z. G. Soos, Phys. Rev. B **66**, 024305 (2002).

[32] *Principles of Luminescence Spectroscopy*, edited by J. R. Lakowicz, 2nd ed. (Kluwer Academic/Plenum, New York, 1999).
[33] E. Runge and E. K. U. Gross, Phys. Rev. Lett. **52**, 997 (1984).
[34] E. K. U. Gross and W. Kohn, Adv. Quantum Chem. **21**, 255 (1990).
[35] E. K. U. Gross, J. F. Dobson, and M. Petersilka, Top. Curr. Chem. **181**, 81 (1996).
[36] A. D. Becke, J. Chem. Phys. **98**, 5648 (1993).
[37] A. Schäfer, H. Horn, and R. Ahlrichs, J. Chem. Phys. **97**, 2571 (1992).
[38] R. Bauernschmitt and R. Ahlrichs, Chem. Phys. Lett. **256**, 454 (1997).
[39] F. Furche and R. Ahlrichs, J. Chem. Phys. **117**, 7433 (2002).
[40] see for current version: http://www.turbomole.de
[41] J. Ridley and M. Zerner, Theor. Chim. Acta **32**, 111 (1973).
[42] N. Mataga and K. Nishimoto, Z. Phys. Chem. (Munich) **13**, 140 (1957).
[43] Z. Shuai and J. L. Brédas, Phys. Rev. B **62**, 15452 (2000).
[44] P. Tavan and K. Schulten, J. Chem. Phys. **85**, 6602 (1986).
[45] P. Tavan and K. Schulten, Phys. Rev. B **36**, 4337 (1987).
[46] Z. Shuai, D. Beljonne, and J. L. Brédas, J. Chem. Phys. **97**, 1132 (1992).
[47] J. R. Heflin, K. Y. Wong, O. Zamani-Khamiri, and A. F. Garito, Phys. Rev. B **38**, 1573 (1988).
[48] D. Guo, S. Mazumdar, S. N. Dixit, F. Kajzar, F. Jarka, Y. Kawabe, and N. Peyghambarian, Phys. Rev. B **48**, 1433 (1993).
[49] E. Zojer, D. Beljonne, P. Pacher, and J. L. Brédas, Chem.-Eur. J. **10**, 2668 (2004).
[50] K. Schmidt, D. Beljonne, J.-L. Brédas, E. Engel, K. Leo, and M. Hoffmann (unpublished).